

Paper:

# Analysis of Topographic Effects in Dynamic Response of a Typical Rocky Populated Slope in Lima, Peru

Carlos Gonzales\*, Shoichi Nakai\*, Toru Sekiguchi\*, Diana Calderon\*\*, Zenon Aguilar\*\*, and Fernando Lazares\*\*

\*Department of Urban Environment Systems, Chiba University

1-33 Yayoi-cho, Inage-ku, Chiba 268-8522, Japan

E-mail: gonzales@chiba-u.jp

\*\*Japan Peru Center for Earthquake Engineering and Disaster Mitigation (CISMID),

Faculty of Civil Engineering, National University of Engineering, Lima, Peru

[Received June 30, 2014; accepted September 22, 2014]

**A currently populated slope in the northeast part of the city of Lima was selected as the target area of this study, with the aim of analyzing the influence of topography on its seismic response. A finite element model was constructed using soil information obtained by microtremor array measurements conducted in flat and sloping areas, and solved for plain strain conditions in the time domain using an input motion developed for the most critical slip model of a simulation for megathrust earthquakes. Results showed that for this typical rocky slope, topographic effects do not have a significant influence on its seismic response, except for areas close to the foot of the slope where, even if soil vibration is restricted, an amplification of the seismic motion is still expected for short period structures.**

**Keywords:** populated slope, microtremor arrays, finite element model, topographic effects

## 1. Introduction

In the last 50 years, Lima, the capital of Peru, has experienced a complex urbanization process in which people from different provinces chose to migrate to the capital looking for a better quality of life. Therefore, these populations relocated not only to areas in the valley of Lima, but also the deserted rocky foothills close to the historical center, resulting in the establishment of new districts with no urban planning policy [1].

The main concern for these new districts is that, in many cases, they are located on steep slopes where little is known about their seismic response to earthquakes. The majority of these locations were populated in the late 1970s, after the last big earthquake struck Lima (October 3, 1974,  $M_w = 8.1$ ), so an analysis of their behavior under strong seismic motions is critical.

To accomplish this objective, a rocky populated slope, located in the northeast part of Lima, was analyzed. In the first stage of this research [2], the dynamic properties of the soil along the slope were estimated, and three seis-

mometers were installed to record seismic events simultaneously: two in the flat area and one about 25 m higher up the slope. The comparison of their respective Fourier spectra, recorded for low magnitude earthquakes, did not show a significant change in the response. Therefore, in the second stage of this study, the decision was made to develop a finite element model of the slope for the case of a megathrust earthquake in Lima. The methodology and analysis considerations for the generated model are discussed in detail in the following sections.

## 2. Area of Study

For the present work, a typical rocky populated slope in the south of the district of Independencia was chosen as the target area (**Fig. 1a**). In general, the city of Lima is built on the alluvial fan formed by the Chillón, Rimac, and Lurín rivers during the Quaternary [3] and the soil in Independencia consists primarily of conglomerate. In addition, due to the proximity of the target slope to the Andean foothills, stiff materials are expected at low depths, and rocky outcroppings, mainly consisting of sandstone and quartzite from the Marcavilca and Herradura geological formations, are evident in upper areas [4].

## 3. Microtremor Campaign

In order to estimate the dynamic properties of the soil substructure for the target slope, seven microtremor array measurements were conducted along a line [2] that included both the flat and the sloping parts of the foothill (line A-A'), with P denoting arrays on the flat area, and S those on the sloping area (**Fig. 1b**). For the computation of reliable dispersion curves, several surface wave methods were applied to the recorded data, and their inversion was performed by the optimization method known as the Genetic Algorithms [5]. Due to the non-uniqueness of the solution, the inversion analysis was conducted five times for each profile (black lines in **Fig. 1c**).

From the estimated shear-wave velocity profiles along

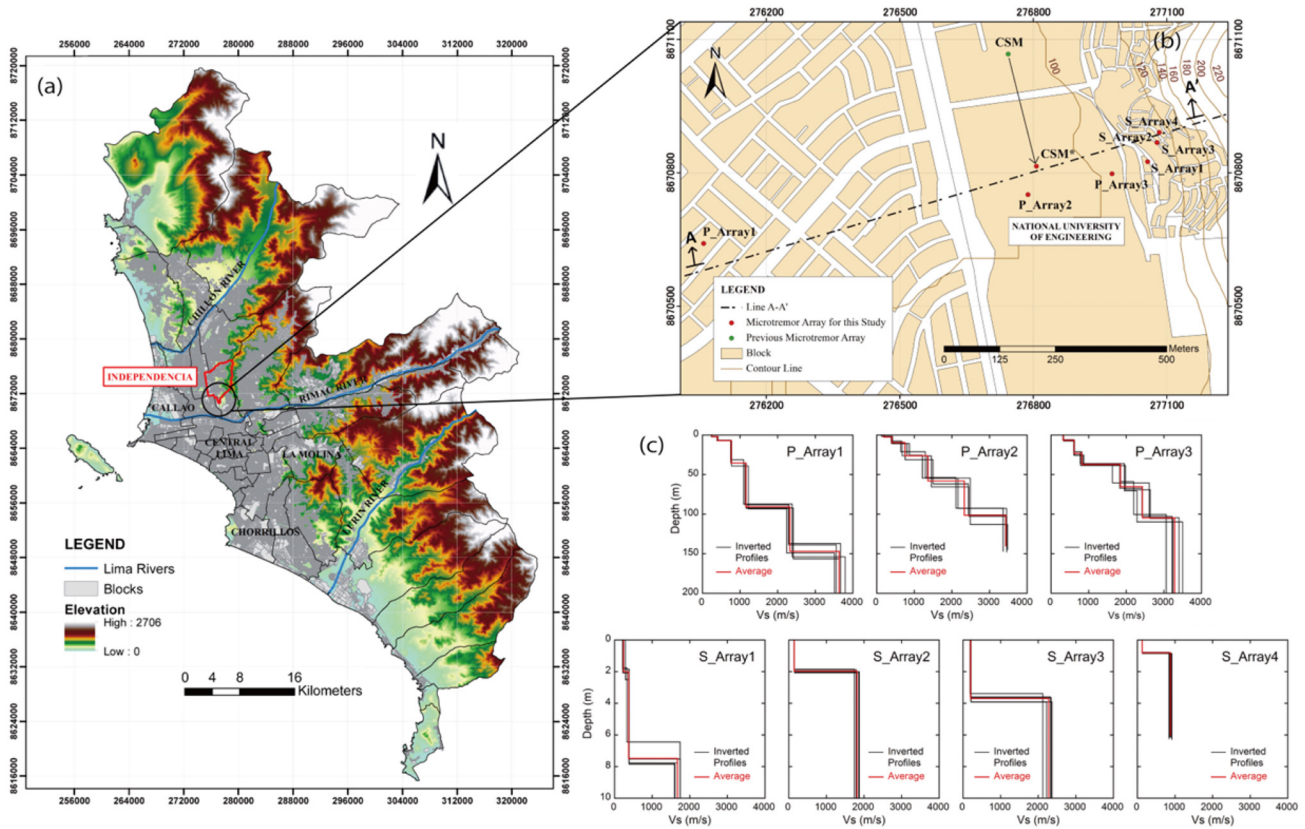


**Fig. 1.** (a) Elevation map of the city of Lima and Independencia district (red line). (b) Location of the microtremor arrays. (c) Calculated shear-wave velocity profiles along line A-A' [2].

line A-A' (Fig. 1c), it can be seen that, for P\_Array1, the depth to the bedrock ( $V_s$  equal to 3000 m/s on average) is about 150 m, and it gradually decreases as the bottom of the slope is approached (P\_Array3). In addition, there is a drastic reduction in the depth to the stiff layers for S\_Array1, indicating that the outcrop of stiff materials must follow a line with a slope of about 50%.

It is important to highlight that for the construction of houses and roads on the slope, the earthmoving technique known as “cut and fill” is commonly adopted, in which the required flat filled areas are generated by the use of land-fill materials that have poor dynamic properties. This is evident for S\_Array2, S\_Array3 and S\_Array4, where the top layer has a shear-wave velocity lower than 200 m/s, and a thickness that ranges from two to four meters. The same pattern can be found for the majority of houses and roads on the slope, with some variations in the thickness of this shallow layer.

## 4. Finite Element Analysis

### 4.1. Dynamic Properties

When developing a finite element model, continuity in the stratification is required, meaning that, for a given layer, the value of its shear-wave velocity ( $V_s$ ) must be kept constant throughout the model. For this purpose, a pattern  $V_s$  structure was calculated from the average of the obtained  $V_s$  values for the flat areas (including CSM\*, which is a slight modification of the original CSM pro-

file obtained in a previous study [6], and was also projected onto line A-A'). This structure was then used as a substructure for profiles in the sloping area, for greater depths than those estimated from linear and small circular microtremor arrays. Attention was paid to the variation of the computed dispersion curves for each profile after changing the values of  $V_s$ , so their thicknesses were adjusted in order to obtain minimum discrepancy from the original results.

The thickness of the shallow layer, consisting of borrowed materials, was assumed to be 2 m for all arrays in the sloping area and, since projections of S\_Array2 and S\_Array3 are almost located in the same position on line A-A', the same  $V_s$  substructure was adopted for these two points. Final values of  $V_s$  and thickness are presented in **Table 1** for the seven microtremor array measurements conducted for this study, and for the CSM\* profile.

In total, seven different types of soil were considered for the finite element model, and their mechanical and dynamic properties are shown in **Table 2**.

### 4.2. Geometry of the Slope

In order to generate the finite element mesh of the slope for its subsequent analysis, satellite images taken by ALOS (Advanced Land Observing Satellite) on October 15, 2008 were used [7]. Altitude information was extracted from the DSM (Digital Surface Model) generated from the PRISM (Panchromatic Remote-sensing Instrument for Stereo Mapping) image of the ALOS data

**Table 1.** Final values of  $V_S$  and thickness for conducted microtremor arrays and CSM\*.

P_Array1		P_Array2		CSM*		P_Array3		
Layer	Thickness (m)	$V_S$ (m/s)						
1	2.0	212	2.0	212	6.5	384	8.0	384
2	5.4	384	7.5	384	15.8	733	26.3	733
3	43.0	733	16.6	733	25.5	1623	28.5	1623
4	59.5	1623	32.0	1623	51.6	2405	41.0	2405
5	55.0	2405	42.3	2405	—	3504	—	3504
6	—	3504	—	3504				

S_Array1		S_Array2		S_Array3		S_Array4		
Layer	Thickness (m)	$V_S$ (m/s)						
1	2.0	176	2.0	176	2.0	176	2.0	176
2	5.5	384	41.0	2405	41.0	2405	37.0	2405
3	28.5	1623	—	3504	—	3504	—	3504
4	41.0	2405						
5	—	3504						

**Table 2.** Dynamic properties for the adopted stratification.

	$\rho$ (kg/m <sup>3</sup> )	$V_S$ (m/s)	$G$ (MPa)	$V_P$ (m/s)	Damping Ratio - $\xi$
Stratum-1	1700	212	77	368	0.030
Stratum-2	1800	384	265	664	0.020
Stratum-3	1800	733	967	1197	0.010
Stratum-4	2200	1623	5794	2508	0.004
Stratum-5	2200	2405	12720	3716	0.003
Stratum-6	2600	3504	31916	5556	0.002
Filled Soil	1500	176	47	367	0.040

through a matching process [8]. The subsequent DSM had a pixel resolution of 5 m, a height resolution of 1 m, and was processed using the GIS (Geographical Information System) software ArcGIS, by drawing a line over the DSM and dividing it into 20-m segments (Fig. 2). Points were created at every vertex of the newly generated segments, and the altitude was estimated by the bilinear interpolation of the information stored in the four nearest cell (pixel) centers to the required point. Finally, points used for the construction of the geometry were carefully selected, since DSM includes not just the ground height, but also the height of features such as buildings and trees.

**4.3. Input Motion**

The simulation conducted by Pulido [9] of a slip scenario for megathrust earthquakes in Lima concluded that there is the potential for generating an earthquake with a moment magnitude of 8.9 off the coast of the capital. As a result of this estimation, synthetic accelerograms were calculated up to the surficial soil for the 8 sites where one-dimensional shear-wave velocity models were available in the capital [6]. For this study, the simulated waveform obtained at CSM for the most critical slip model was assumed to be the same as for CSM\*, owing to its proximity to line A-A'. This waveform was therefore deconvoluted in order to obtain the input motion at the bottom

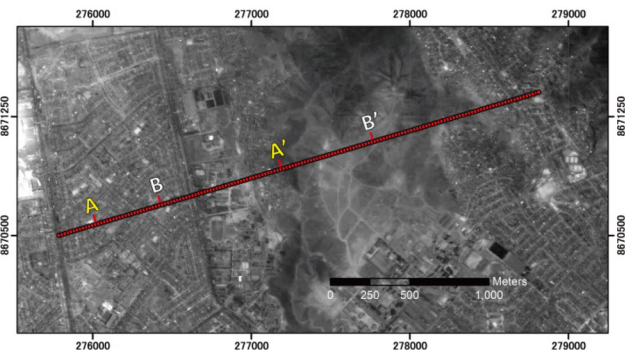


**Fig. 2.** Points along lines A-A' and B-B' over the Digital Surface Model from the ALOS satellite image.

layer of the model ( $V_S = 3504$  m/s). Fourier spectra and waveforms for both surface and deconvoluted motions are shown in Fig. 3.

Equivalent linear analysis was performed in order to clarify if the nonlinear behavior of soils could affect the CSM profile when the deconvoluted input motion is applied. For this type of analysis, a set of  $G/G_{max}$  and hysteretic damping curves, developed by EPRI [10] and used by Walling [11] for cohesionless soils, were adopted due to the lack of this type of information for Lima. Similar values for both PGA and PGV were obtained for linear and equivalent linear cases, allowing us to conclude that nonlinear behavior does not have a significant influence on the variation of the response. Therefore, calculations for the slope model were made considering a linear response. Fourier and response spectra for both cases, as well as transfer functions, are shown in Fig. 4.

**4.4. Analysis Considerations**

**4.4.1. Time Domain Analysis**

In dynamic analysis, when including damping, the equation of motion is typically written in the form

$$M\ddot{u} + C\dot{u} + Ku = -M\ddot{u}_e, \dots \dots \dots (1)$$

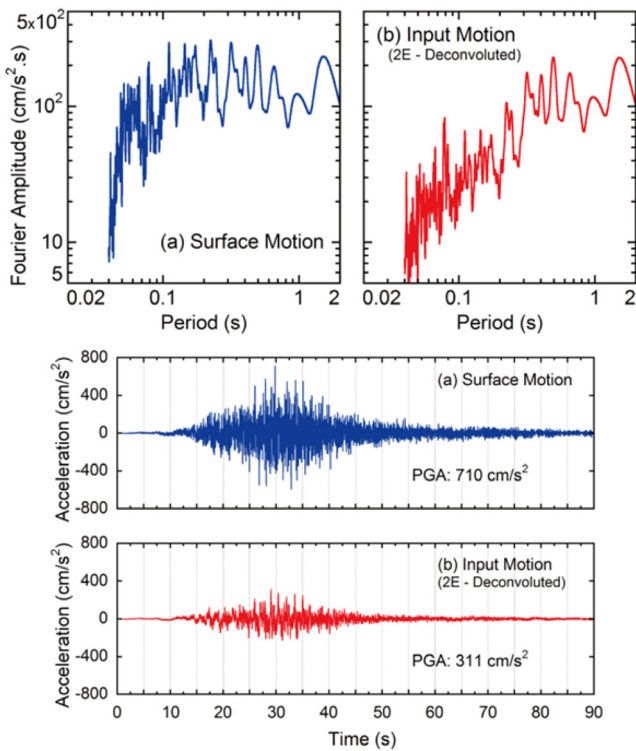


**Fig. 3.** Fourier spectra and time-histories for (a) surface motion and (b) deconvoluted input motion.

where  $\mathbf{M}$  is the mass matrix,  $\mathbf{C}$  the viscous damping matrix,  $\mathbf{K}$  the stiffness matrix,  $\ddot{\mathbf{u}}$  the acceleration vector,  $\dot{\mathbf{u}}$  the velocity vector,  $\mathbf{u}$  the displacement vector,  $\ddot{u}_e$  the seismic acceleration, and  $\mathbf{M}\ddot{u}_e$  the inertia vector. Eq. (1) was solved numerically by means of the Newmark- $\beta$  method [12] in which  $\Delta t$ , the time interval, and the parameter  $\beta$  were assumed to be 0.002 s and 0.25, respectively.

#### 4.4.2. Attenuation Type

In the time domain analysis, the viscous damping matrix,  $\mathbf{C}$ , is frequency dependent. In the original formulation proposed by Rayleigh and Lindsay [13],  $\mathbf{C}$  is assumed to be proportional to mass and stiffness matrices as follows:

$$\mathbf{C} = \alpha_R \mathbf{M} + \beta_R \mathbf{K}, \quad \dots \dots \dots (2)$$

The coefficients  $\alpha_R$  and  $\beta_R$  can be computed using two significant natural modes,  $m$  and  $n$ , by means of the following equation:

$$\begin{bmatrix} \xi_m \\ \xi_n \end{bmatrix} = \frac{1}{2} \begin{bmatrix} \frac{1}{\omega_m} & \omega_m \\ \frac{1}{\omega_n} & \omega_n \end{bmatrix} \begin{Bmatrix} \alpha_R \\ \beta_R \end{Bmatrix} = \frac{1}{2} \begin{bmatrix} \frac{1}{2\pi f_m} & 2\pi f_m \\ \frac{1}{2\pi f_n} & 2\pi f_n \end{bmatrix} \begin{Bmatrix} \alpha_R \\ \beta_R \end{Bmatrix}, \quad \dots \dots \dots (3)$$

where  $\xi_m$ ,  $\xi_n$  and  $f_m$ ,  $f_n$  are damping ratios and frequencies, respectively, for the two corresponding modes  $m$  and  $n$ . Since the damping ratio is known to be frequency independent, equal values for modal damping ratios,  $\xi$ , are

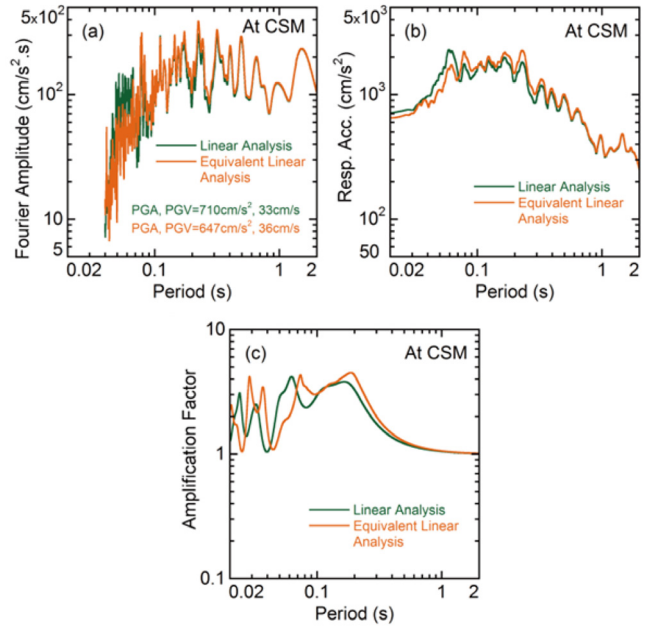


**Fig. 4.** (a) Fourier spectra, (b) acceleration response spectra and (c) transfer functions for linear and equivalent linear cases.

specified for the two modes. Then, after solving Eq. (3),

$$\alpha_R = \frac{4\pi f_m f_n \xi}{(f_m + f_n)} \quad \dots \dots \dots (4)$$

and 
$$\beta_R = \frac{\xi}{\pi(f_m + f_n)}, \quad \dots \dots \dots (5)$$

The analysis was performed for several trials of the set of frequencies  $f_m$  and  $f_n$ , in order to find the closest PGA possible to that for the EW component (chosen due to the orientation of line A-A') of the simulated accelerogram at CSM\* (assumed to be the same as for CSM) developed for the most critical slip model, following the recommendations given in [14] and [15]. Also, comparisons of both Fourier and response spectra, for 5% damping of the synthetic and output waveforms from the finite element model at CSM\*, were used for the selection purposes. After several assumptions, the most suitable  $f_m$  and  $f_n$  were found at 3.33 Hz and 25 Hz, respectively (**Fig. 5**).

#### 4.4.3. Finite Element Model

A commercial program known as Soil Plus was utilized for construction of the two-dimensional finite element model of the target populated slope and its subsequent dynamic analysis.

Boundaries and thicknesses of the seven strata were clearly defined from the shear-wave velocity profiles in the flat area. Transitions of materials in the sloping area were modeled based on the fact that layers with a low shear-wave velocity gradually disappear approaching the foot of the slope, because of the outcropping of stiff rocky materials. During the microtremor field work on the slope, it was evident that fresh rock appears just above the currently inhabited areas. An approximate location for

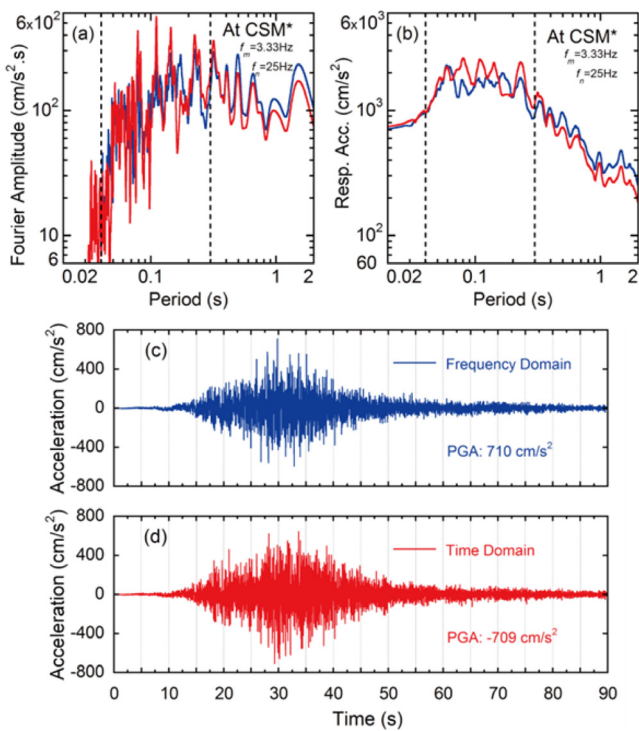


**Fig. 5.** (a) Fourier spectra, (b) acceleration response spectra, and (c) waveforms for the frequency domain and (d) the time domain (FEM): results at CSM\* ( $f_m = 3.33$  Hz and  $f_n = 25$  Hz).

this outcropping was chosen with the help of the ALOS satellite and Google Earth images.

In order to generate the mesh for each stratum, their respective surrounding edges were divided into control points with increased spacing at greater depths. In general, quadrilateral shapes were used, but in specific cases, such as in the transition to outcropping materials, triangular elements were generated.

The problem was solved for plain strain conditions, in which the thickness perpendicular to the analysis plane was equal to 1 m for all soil elements. In order to save computation time and avoid the generation of an unnecessarily large number of degrees of freedom, the slope model was reduced from the original drawn line (red dots in Fig. 2) to the central-third portion represented by line B-B'. In total, 7996 planar elements were generated for the two-dimensional model, and their distribution for each assumed stratum, as well as their graphical representation, is shown in Fig. 6.

#### 4.4.4. Boundary Conditions

Compression and shear dampers were placed at the sides and bottom of the model. Depending on the type of force applied, damper constants ( $C_c$  and  $C_s$ ) were calculated from the following expressions:

$$C_c = \rho V_P A \quad \dots \dots \dots (6)$$

and  $C_s = \rho V_S A, \dots \dots \dots (7)$

where  $\rho$  is the density,  $V_P$  the compressional-wave velocity,  $V_S$  the shear-wave velocity of the layer to which the

damper is attached, and  $A$  its area of influence. Additionally, in order to develop a consistent model, free ground elements with large mass were placed on the opposite sides of the model with a thickness equal to 100000 m. A scheme of dampers and free ground elements is also shown in Fig. 6.

## 5. Analysis Results

The distribution of absolute values of peak acceleration for horizontal motion, for the entire slope model, is presented in Fig. 7a. This figure shows that amplification of the response is evident for surface layers in the flat areas, whereas no larger values are found for the sloping areas of the model. In addition, Fig. 7b shows a close-up view that includes the foot of the slope and regions assumed to be covered by borrowed soil.

Waveforms were extracted for three points along the slope: point a, close to the foot of the slope; point b, in the center of the populated areas covered by borrowed soil; and point c, in the region where full outcropping of fresh rock is assumed to start. In addition, a one-dimensional amplification analysis was conducted for each of these three points, in which a soil column with the same mechanical and dynamic properties was analyzed and additionally solved for the time domain.

Results (Fig. 8) show that the largest PGA occurs at point a, with an acceleration value ( $602 \text{ cm/s}^2$ ) which only differs by approximately  $100 \text{ cm/s}^2$  from the one obtained for CSM\* (Fig. 3a). This contrasts with lower values found by FEM analysis for the other two points. Moreover, in Fig. 8a it is evident that Fourier amplitudes for the FEM case are lower than those obtained from one-dimensional analysis for points a, b, and c. These results are a consequence of the apparent restricted vibrations close to the foot of the slope caused by the stiff rocky hill next to the flat area. On the other hand, recent studies [16] have concluded that PGA and response acceleration are key factors in the estimation of structural damage in Peru. Therefore, comparisons of acceleration response spectra (Fig. 8b) are shown, and a peak can be observed for points a and b for periods close to 0.07 s. Since one-story masonry houses and other essential structures (schools, community centers, etc.) are extensive in these areas, an increase in their seismic response is expected due to the similarity of their natural periods of vibration to the value given above [17].

Results at this stage also confirm the fact that nonlinear behavior of soils does not affect the response of the target slope, since PGV values ( $24 \text{ cm/s}$  on average) for points along the slope are fairly low to consider this effect.

## 6. Conclusions

This study aimed to analyze the dynamic response of a typical rocky populated slope in the city of Lima, and the possibility of finding amplification due to topographic

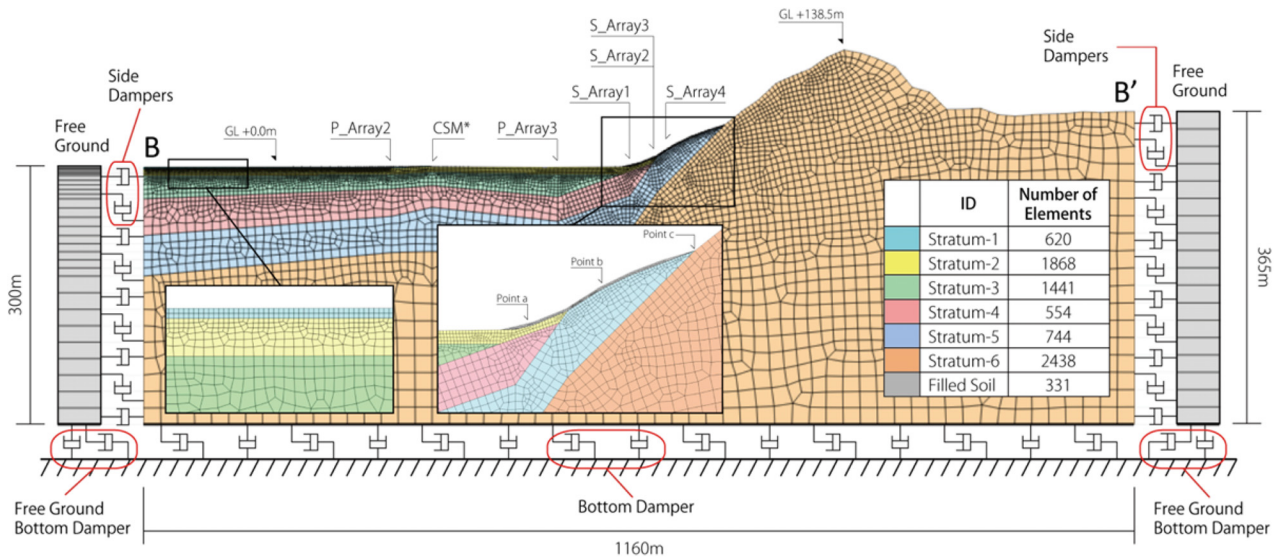


Fig. 6. Two-dimensional finite element model of the target slope.

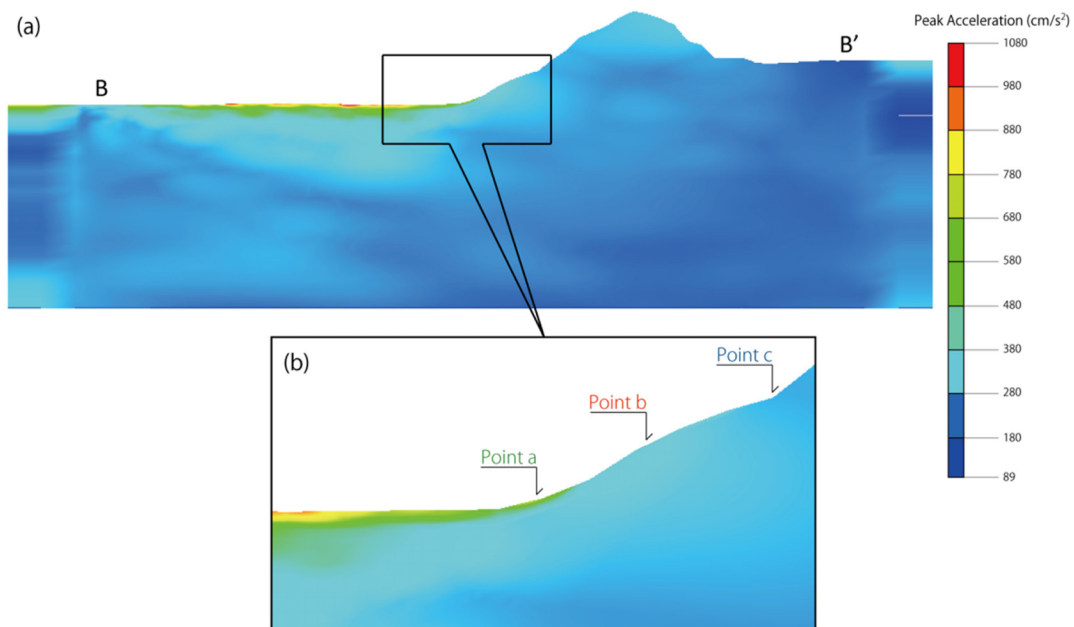


Fig. 7. Distribution of the peak acceleration in the horizontal direction for (a) the entire finite element model and (b) the sloping areas.

effects. The following conclusions can be drawn from this study.

1. An equivalent linear analysis, carried out for the soil column corresponding to the CSM profile, demonstrated that the effect of nonlinearity does not produce a significant influence on the seismic response. Therefore, analysis of the complex slope model was performed for the linear case.
2. A mathematical model was developed by means of the finite element method (FEM) and solved for the time domain, allowing us to obtain time-histories for several points on the sloping area. Comparisons of the results for the FEM and one-dimensional cases have shown that soil vibration close to the foot of

the slope may be restricted when considering the effect of the stiff rocky hill. Results also indicated that a larger response is evident for regions close to the foot of the slope, for periods in the vicinity of 0.07 s. This period coincides with the expected natural period of one-story masonry buildings that are extensive in these areas, meaning that they may be significantly affected by strong motions of large magnitude. This difference in the response seems to be influenced more by the shear-wave velocity substructure of the slope than by topography effects.

Further analyses of other populated slopes throughout the city are recommended, in order to develop a general understanding of their seismic response, since geomet-

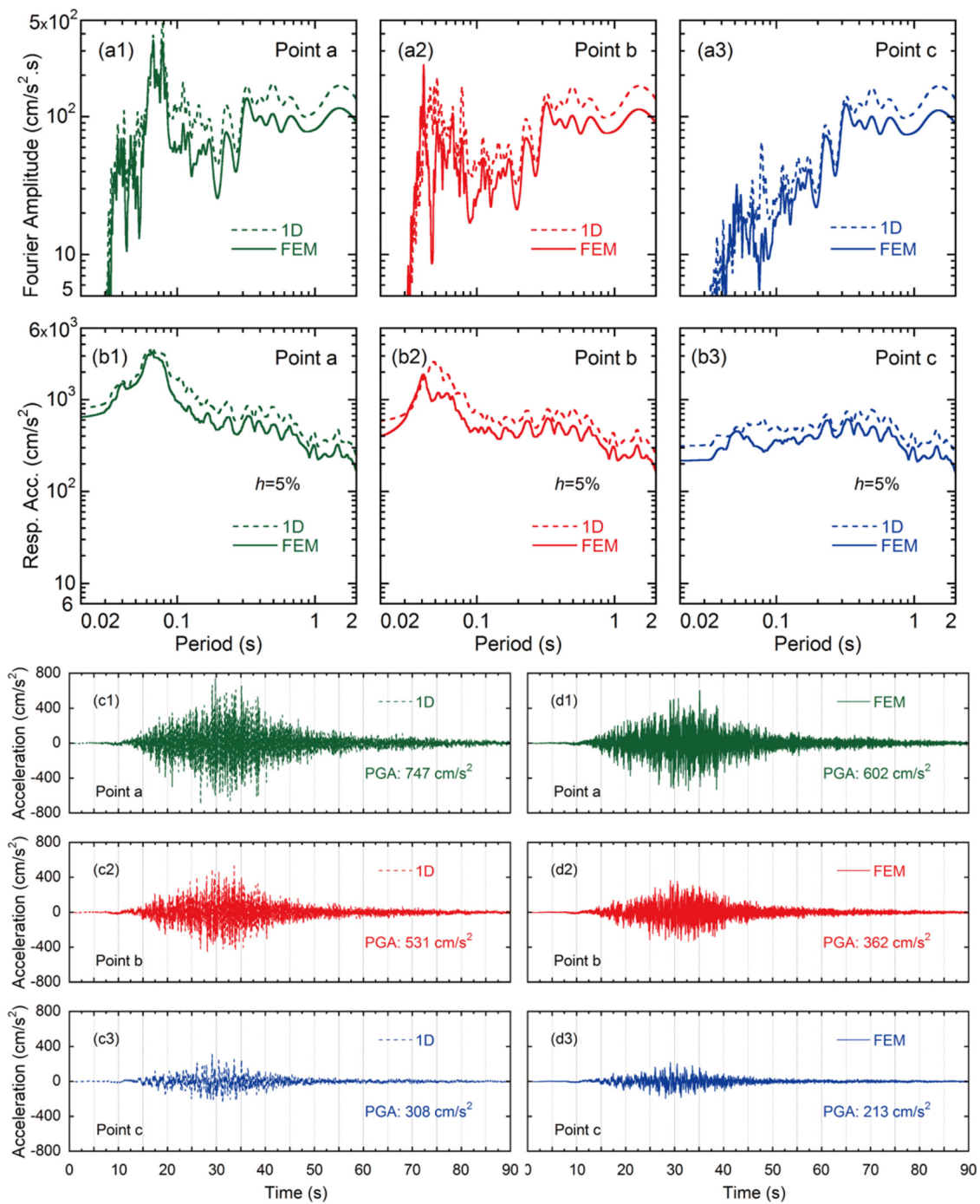


**Fig. 8.** Comparison of the (a1–3) Fourier spectra, (b1–3) acceleration response spectra for one-dimensional and FEM analyses. Acceleration time-histories for (c1–3) one-dimensional and (d1–3) FEM analyses.

ric and geotechnical conditions may differ from the target slope considered for this study that can be assumed to be typical only for the stiff rocky slopes in the north region of Lima.

**Acknowledgements**

This work was developed within the framework of the SATREPS project on “Enhancement of Earthquake and Tsunami Disaster Mitigation Technology in Peru,” under the patronage of the Japan Science and Technology Agency (JST) and the Japan International Cooperation Agency (JICA).

The authors would like to express their gratitude to these agencies and to the research assistants in CISMID who helped in the completion of the study.

**References:**

- [1] J. Matos, *Las Migraciones Campesinas y el Proceso de Urbanización en el Perú*, UNESCO, 1990 (in Spanish).
- [2] C. Gonzales, S. Nakai, T. Sekiguchi, D. Calderon, Z. Aguilar, and F. Lazares, "Estimation of the Dynamic Properties and Seismic Response of a Populated Slope in Lima, Peru," *Journal of Disaster Research*, Vol.9, No.1, pp. 17-26, 2014.
- [3] Z. Aguilar, "Seismic Microzonation of Lima," *Japan-Peru Workshop on Earthquake Disaster Mitigation*, Japan-Peru Center for Earthquake Engineering Research and Disaster Mitigation (CISMID), Faculty of Civil Engineering, National University of Engineering, Lima, Peru, 2005.
- [4] O. Palacios, J. Caldas, and Ch. Vela, "Geología de los Cuadrangulos de Lima, Lurin, Chancay y Chosica," *The Geological, Mining and Metallurgical Institute of Peru*, pp. 25-29, 1992 (in Spanish).
- [5] H. Yamanaka and H. Ishida, "Application of the Genetic Algorithms to an Inversion of Surface-Wave Dispersion Data," *Bulletin of Seismological Society of America*, Vol.86, No.2, pp. 436-444.
- [6] D. Calderon, "Dynamic characteristics of the soils in Lima, Peru, by estimating shallow and deep shear-wave velocity profiles," *Graduate School of Engineering, Chiba University, Japan*, 2012.
- [7] M. Matsuoka, H. Miura, S. Midorikawa, and M. Estrada, "Extraction of Urban Information for Seismic Hazard and Risk Assessment in Lima, Peru Using Satellite Imagery," *Journal of Disaster Research*, Vol.8, No.2, pp. 328-345, 2013.
- [8] J. Takaku and T. Tadano, "PRISM on-Orbit Geometric Calibration and DSM Performance," *IEEE Transaction on Geoscience and Remote Sensing*, Vol.47, No.12, pp. 4060-4073, 2009.
- [9] N. Pulido, "Earthquake rupture and slip scenarios for Central Andes Peru, and strong motion simulations for Lima," *National Research Institute for Earth Science and Disaster Prevention (NIED)*, 2013.
- [10] Electric Power Research Institute (EPRI), "Guidelines for Determining Design Basis Ground Motions. Volume 1: Method and Guidelines for Estimating Earthquake Ground Motion in Eastern North America," *Technical Report*, 1993.
- [11] M. Walling, W. Silva, and N. Abrahamson, "Nonlinear Site Amplification Factors for Constraining the NGA Models," *Earthquake Spectra*, Vol.24, No.1, pp. 243-255, 2008.
- [12] N. Newmark, "A Method of Computation for Structural Dynamics," *Journal of the Engineering Mechanics Division*, Vol.85, pp. 67-94, 1959.
- [13] J. Rayleigh and R. Lindsay, *The Theory of Sound*, 1<sup>st</sup> American Ed. New York, Dover Publications, 1945.
- [14] Y. Hashash and D. Park, "Viscous damping formulation and high frequency motion propagation in non-linear site response analysis," *Soil Dynamics and Earthquake Engineering*, Vol.22, pp. 611-624, 2002.
- [15] D. Park and Y. Hashash, "Soil damping formulation in nonlinear time domain site response analysis," *Journal of Earthquake Engineering*, Vol.8, No.2, pp. 249-274, 2004.
- [16] L. Quiroz, "Evaluation of Seismic Performance of Residential Buildings in Lima, Peru: A Case Study of Buildings Constructed with Thin RC Walls and Confined Masonry Walls," *Graduate School of Engineering, Division of Architecture and Urban Science, Department of Urban Environment Systems, Chiba University, Doctoral Thesis*, 2014.
- [17] R. Proaño and C. Zavala, "Estimation of the seismic response of structures based on SDOF systems for calculation of Seismic Vulnerability," *Proceedings of the XIV National Conference of Civil Engineering*, Iquitos, Peru, Paper No.EM-38, p. 12, 2003 (in Spanish).



**Name:**

Carlos Gonzales Trujillo

**Affiliation:**

Ph.D. Student, Department of Urban Environment Systems, Chiba University

**Address:**

1-33, Yayoi-cho, Inage-ku, Chiba 268-8522, Japan

**Brief Career:**

2009 B.Sc. Civil Engineer, Faculty of Civil Engineering, National University of Engineering (UNI), Lima, Peru

2010-2011 Research Assistant, Japan-Peru Center for Earthquake Engineering Research and Disaster Mitigation (CISMID)

2012-2014 Master of Engineering, Chiba University

2014- Ph.D. student, Chiba University

**Selected Publications:**

- "Estimation of the Dynamic Properties and Seismic Response of a Populated Slope in Lima, Peru," *Journal of Disaster Research*, Vol.9, No.1, pp. 17-26, Feb. 2014.